We are IntechOpen, the world's leading publisher of Open Access books
Built by scientists, for scientists

4,800
Open access books available

122,000
International authors and editors

135M
Downloads

154
Countries delivered to

Our authors are among the
TOP 1%
most cited scientists

12.2%
Contributors from top 500 universities

CLARIVATE ANALYTICS
BOOK CITATION INDEX
INDEXED

WEB OF SCIENCE™

Selection of our books indexed in the Book Citation Index
in Web of Science™ Core Collection (BKCI)

Interested in publishing with us?
Contact book.department@intechopen.com

Numbers displayed above are based on latest data collected.
For more information visit www.intechopen.com

Solid Particle Erosion on Different Metallic Materials

Juan R. Laguna-Camacho, M. Vite-Torres,
E.A. Gallardo-Hernández and E.E. Vera-Cárdenas

Additional information is available at the end of the chapter

1. Introduction

Testing on ferrous and non-ferrous materials has been widely carried out to study their erosion resistance. Venkataraman & Sundararajan [1] conducted a study about the solid particle erosion of copper at a range of low impact velocities. In this particular case, the eroded surface was completely covered with the erosion debris in the form of flakes or platelets. These flakes appeared to be completely separated or fractured from the material surface and were flattened by subsequent impacts. For this reason, it was concluded that at low impact velocities the erosion damage was characterized mainly by lip or platelet fracture whereas it was distinguished with lip formation (rather than its subsequent fracture) at higher impact velocities.

Additionally, studies on the erosion behaviour of AISI 4140 steel under various heat treatment conditions was investigated by Ambrosini & Bahadur [2]. In this work, the investigation was concentrated on the effect of various microstructures and mechanical properties on the erosion resistance. A constant velocity of 50 m/s was used for all the erosion tests. The target was impacted at an angle of 30º to the specimen surface, the particle feed rate was 20 g/min, SiC particles, 125 μm in size, were used as the abrasive. From the results, it was concluded that erosion rate increases with increasing hardness and ultimate strength, but decreases with increasing ductility. In this particular work, the heat treatment with the optimum combination of erosion resistance and mechanical properties was oil quenching followed by tempering in the temperature range 480-595 ºC for 2 h. In addition, SEM studies presented severe plastic deformation in the eroded zones together with abrasion marks, indicating that material subjected to erosion initially undergoes plastic deformation and is later removed by abrasion.

Harsha & Bhaskar [3] carried out research to study the erosion behaviour of ferrous and non-ferrous materials and also to examine the erosion model developed for normal and oblique impact angles by Hutchings [4]. The materials tested were aluminium, brass, copper, mild steel, stainless steel and cast iron. They determined from the SEM studies that the worn surfaces had revealed various wear mechanisms such as microploughing, lip formation, platelet, small craters of indentation and microcracking.

In addition to these studies, Morrison & Scattergood [5] carried out erosion tests on 304 stainless steel. In this work, it was concluded from the SEM observations that similar morphologies for low and high impact angles could be observed in ductile metals when they were subjected to the impact of sharp particles. The surfaces displayed a peak-and-valley topology together with attached platelet mechanisms. In addition, the physical basis for a single-mechanism to erosion in ductile metals was considered to be related to shear deformations that control material displacement within a process zone for a general set of impact events producing at all impact angles. These events included indentation, ploughing and cutting or micromachining. In respect to the effect of the erodent particle shape on solid particle erosion, Hutchings showed differences in eroded surfaces due to a shape particle effect [6]. It was observed that the shape of abrasive particles influences the pattern of plastic deformation around each indentation and the proportion of material displaced from each indentation, which forms a rim or lip. More rounded particles led to less localized deformation, and more impacts were required to remove each fragment of debris.

Liebhard & Levy [7] conducted a study related to the effect of erodent particle characteristics on the erosion of 1018 steel. Spherical glass beads of four different diameter ranges between 53-600 μm and angular SiC of nine different diameter ranges between 44-991 μm were the erodents. The particle velocities were 20 and 60 m/s, an impact angle of 30º was used to conduct all the tests and the feed rate was varied from 0.6 to 6 g/min. The results showed that there was a big difference in the erosivity of the spherical and angular particles as a function of particle size. Angular particles generally were an order of magnitude more erosive than spherical particles. In addition, the erosivity of spherical particles increased with particle size to a peak and then decrease at even larger particle sizes. In respect to angular particle erosivity, it was increased with particle size to a level that became nearly constant with size at lower velocities, but increased continuously at higher particle velocities. Lower flow rates caused more mass loss than higher flow rates for both spherical and angular particles.

In this work, the performance of different metallic materials has been analyzed. The aim of this experimentation was essentially to know the behavior of these materials against solid particle erosion and compare their erosion resistance. In addition, the functionality of both, the rig and the velocity measurement method was evaluated.

2. Experimental details

2.1. Specimens

The materials employed to conduct the tests were 4140 and 1018 steels, stainless steel 304, 316 and 420, aluminium 6061, brass and copper. The test surface of each specimen was

ground using SiC emery paper grade 1200. The average roughness (R_a) in each specimen before testing was 1 μm. The samples had a rectangular shape with dimensions of 50 x 25 mm² and 3 mm in thickness. The abrasive particle used was silicon carbide (SiC) of an angular shape, as seen in Figure 1, with a particle size of 420-450 μm [8]. Table 1 presents the chemical composition of the materials used in the erosion tests whereas Table 2 shows the hardness of the materials. Microhardness values were obtained by calculating an average value, 10 different points were measured. The applied load was 100gf.
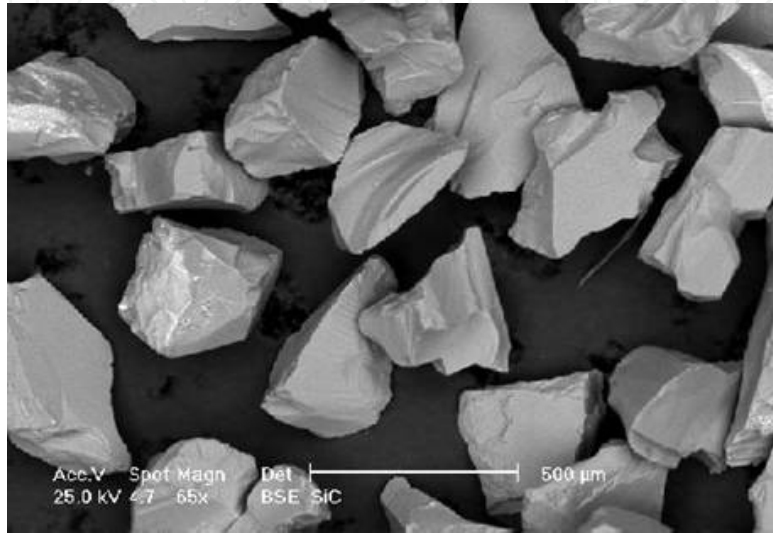
Figure 1. Size and morphology of the abrasive particles [8]

Material	C	Si	Mn	Mg	P máx.	S máx.	Cr	Ni	V	Cu	Mo	Pb	Zn	Ti
4140	0.38-0.43	0.15-0.35	0.75-1.00	-	0.035	0.040	0.80-1.10	-		-	0.15-0.25		-	-
1018	0.15-0.20	0.15-0.35	0.60-0.90	-	0.040	0.50	-	-	-	-	-		-	-
304	0.08	1.00	2.00	-	-	-	16.00 - 18.00	8.00-10.50		-	-		-	-
316	0.08	1.00	2.00	-	-	-	16.00 - 18.00	10.00 - 14.00		-	2.00-3.00		-	-
420	0.38	0.40	0.45	-	-	-	13.60	-	0.30	-	-		-	-
Aluminium 6061	0.40-0.82	-	0.15 Máx.	0.80-1.20	-	-	0.04-0.35			0.15-0.40	-		0.25 Máx.	0.15 Máx.
Brass	-	-	-	-	-	-	-	-	-	55.84	-	0.05 Máx.	Rem.	-
Copper	-	-	-	-	-	-	-	-	-	87.66	-	0.05 máx.	Rem.	-

Table 1. Chemical composition of materials

Material	Vickers Hardness (HV)
4140	280
1018	230
AISI 304	160
AISI 316	150
AISI 420	200-240
Aluminium 6061	130
Brass	228
Copper	161

Table 2. Hardness

2.2. Test procedure

The apparatus used to carry out the erosion tests is similar to that presented in the ASTM G76-95 test standard [8-10]. Figure 2 shows a schematic diagram of the rig that was developed. In this device, the particles of silicon carbide (SiC) were accelerated from a nozzle by using a compressed air stream that caused them to impact the surface of the material.

The materials were eroded in a time period of 10 min, although each sample was removed every 2 min to determine the amount of mass lost. The specimen holder could be rotated to be impinged at different incident angles (30º, 45º, 60º, 75º and 90º). These angles were selected to evaluate the materials at both low and high impact angles and to determine if the behavior of these materials was similar to the conventional materials that were used in other erosion studies [1-4]. A particle velocity of 24 ± 2 m/s and a constant abrasive flow rate of 0.7 ± 0.5 g/min were used to reduce the effects of interaction between the incident particles and the rebounding particles. The reduction of this effect was usually accomplished at lower impact angles such as 30° and 45°, where the abrasive particles commonly impacted the material, slid along the surface, and then fell away. However, a greater level of interaction between the particles was observed at 90°. The measurements of particle velocity were carried out by using an opto-electronic system.

In all of the tests, specimens were located 10 ± 1 mm from the end of the glass nozzle. The nozzle had the following dimensions: a 4.7 mm internal diameter, a 6.3 mm external diameter and 260 mm length. The room temperature was between 35 and 40º C. The specimens were weighed using an analytical balance with an accuracy of ± 0.0001 g, before the start of each test and were removed every 2 min, cleaned in an ultrasonic cleaning device using ethanol and weighed again to determine the mass lost. Subsequently, micrographs of eroded surfaces were obtained using a scanning electron microscope (SEM) to analyze and identify the possible wear mechanisms involved.
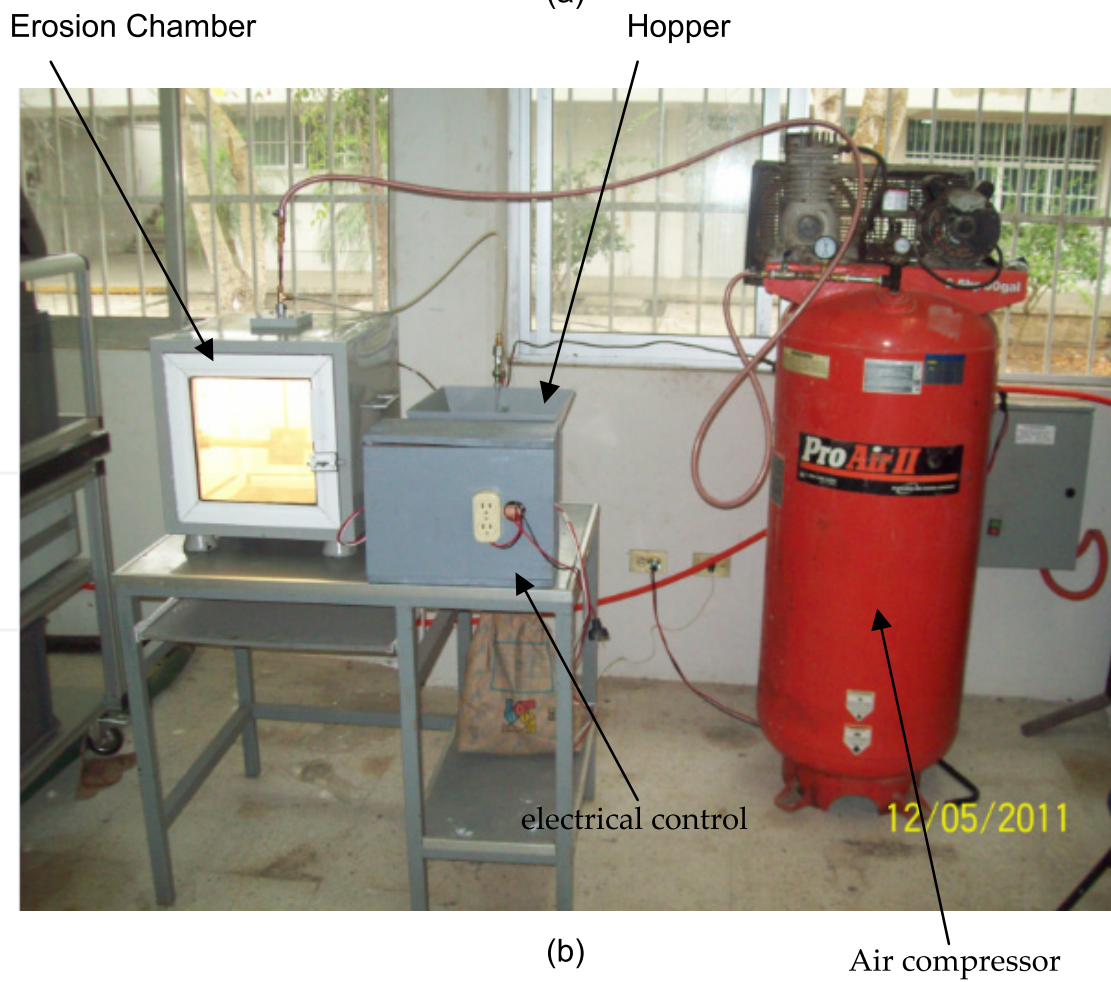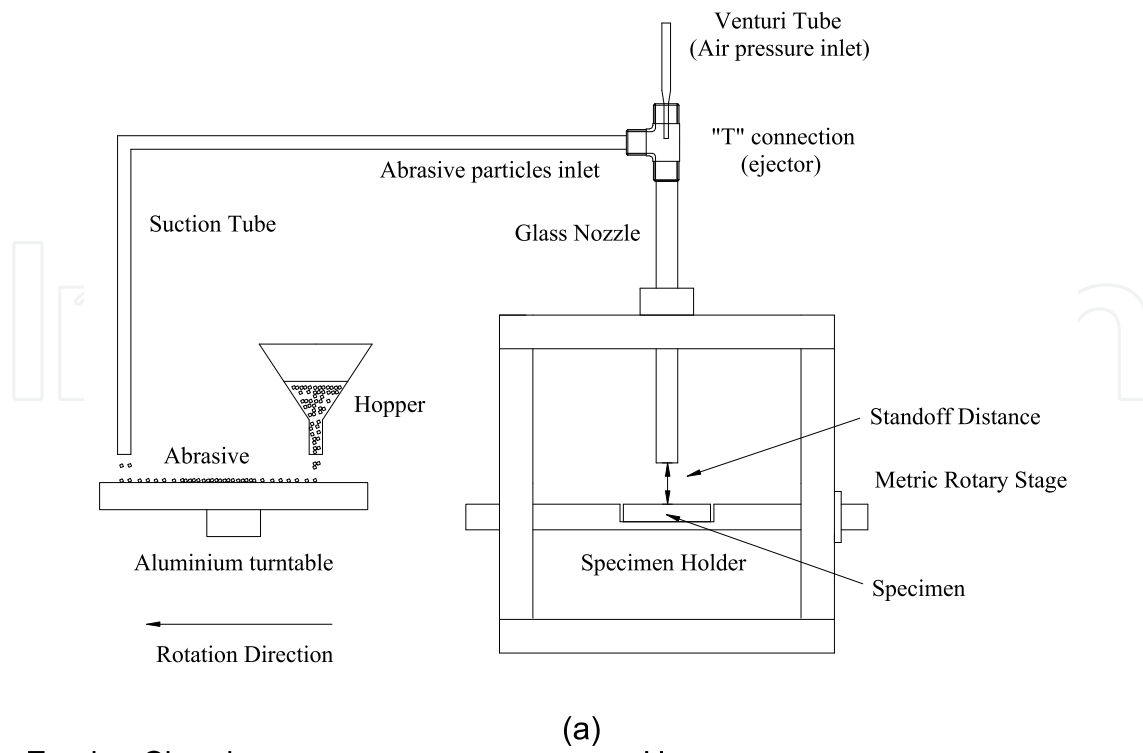
(a)

(b)

Figure 2. (a) Schematic Diagram of erosion rig developed, (b) Experimental setup [8]

2.3. Velocity measurement method

The particle velocity was measured with an opto-electronic flight-timer similar to that described by Kosel and Anand [11, 12]. This system offers the possibility to measure the particle velocity in an accurate mode and the design does not request high costs. It is practical and flexible in relation to the equipment that can be used to conduct the measurements, for instance, the oscilloscope, the emitters and detectors, etc. It must be mentioned because other equipment such as a high speed camera are expensive and result more difficult to obtain them to conduct a research project. The uncertainties of this particular system are that the measurements are not as consistent as expected. In certain cases, it is necessary to use more abrasive particles to obtain a signal and finally to complete the measurement process. In this specific work, several air pressures, from 0.35 kg/cm² (5 psi) to 3.86 kg/cm² (55 psi) were used to conduct the tests. It was concluded that a higher pressure and therefore a higher particle velocity gave better results. Due to this fact, 3.86 kg/cm² (55 psi) equivalent to 24 ± 2 m/s was the value chosen to carry out the erosion tests. Signals more consistent and clear were obtained using this particle velocity.

The velocity measurement method is mainly composed of two infra-red emitters and detectors held by a rectangular plastic block as observed in the schematic diagram in Figure 3a. A few abrasive particles pass through a glass tube attached at the end of the nozzle and are recognized by both light beams producing the signals that are processed through an amplification system connected to an oscilloscope. It is possible to determine the real time travelled by a few abrasive particles using the two signals, 1 and 2. The standard distance between signals was 10 ± 1 mm. Flight time data were continuously collected and stored. An average particle velocity was reached after 20 measurements. The set-up developed is shown in Figure 3b. As observed, the infra-red emitters were set on each side to ensure that most of the abrasive particles were monitored when passing through the glass tube. Finally, an example of the signals received directly in the oscilloscope is presented in Figure 3c.

3. Test results

3.1. Wear mechanisms
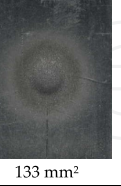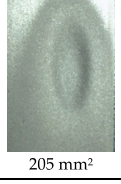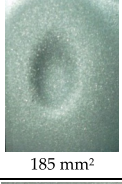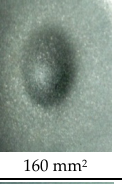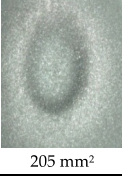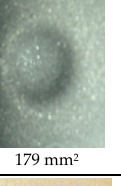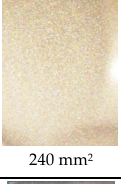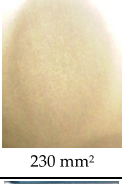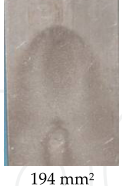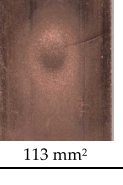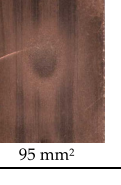
In Figure 4, it is possible to observe the wear scars obtained for all the tested materials at different incident angles. The wear scar area is reduced as the impact angle is increased. It has an elliptical shape at 30° and 45º whereas a roughly circular shape is observed at 60º and 90°. This can be related to the impact geometry which modifies the orientation of the specimen when it is positioned at different incident angles. In the schematic diagram shown in Figure 5a and b, A, represents the wear scar independently of the halo effect distinguished by the dashed lines. Due to this fact, the wear scar commonly shows an elliptical shape at incidence angles lower than 45º due to a higher divergence of the particle stream. A circular shape is often observed at higher impact angles near or at 90º as observed commonly in other erosion studies [13-17]. In both cases, the plume of abrasive particles is concentrated in the central part of the stream. All materials showed clearly the halo effect

[18], mentioned above, which is represented by a secondary erosion damage zone. The estimated area of the erosive scars including the halo effect is presented in photographs in Figure 4.

(a)   (b)

(c)
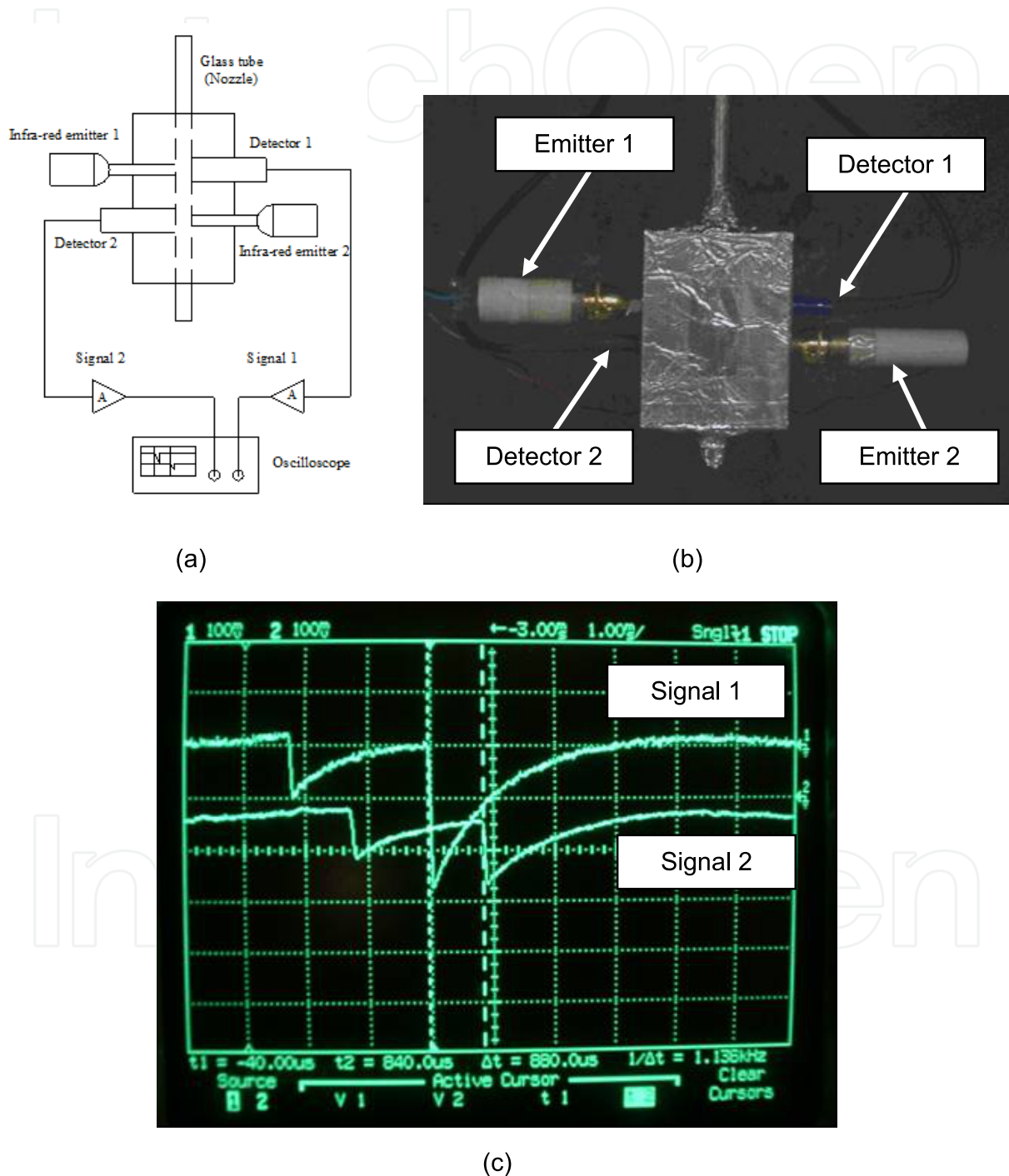
Figure 3. (a) Schematic diagram of set-up, (b) Real set-up developed, (c) Signals 1 and 2 processed in the oscilloscope

Material	30º	45º	60º	90º
4140 steel	226 mm²	220 mm²	201 mm²	177 mm²
1018 steel	170 mm²	170 mm²	153 mm²	133 mm²
304 stainless steel	205 mm²	185 mm²	160 mm²	153 mm²
316 stainless steel	230 mm²	205 mm²	186 mm²	179 mm²
420 stainless steel	240 mm²	230 mm²	225 mm²	215 mm²
6061 aluminium	210 mm²	194 mm²	145 mm²	130 mm²
Brass	220 mm²	188 mm²	113 mm²	113 mm²
Copper	188 mm²	184 mm²	113 mm²	95 mm²

Figure 4. Erosion Damage on tested materials
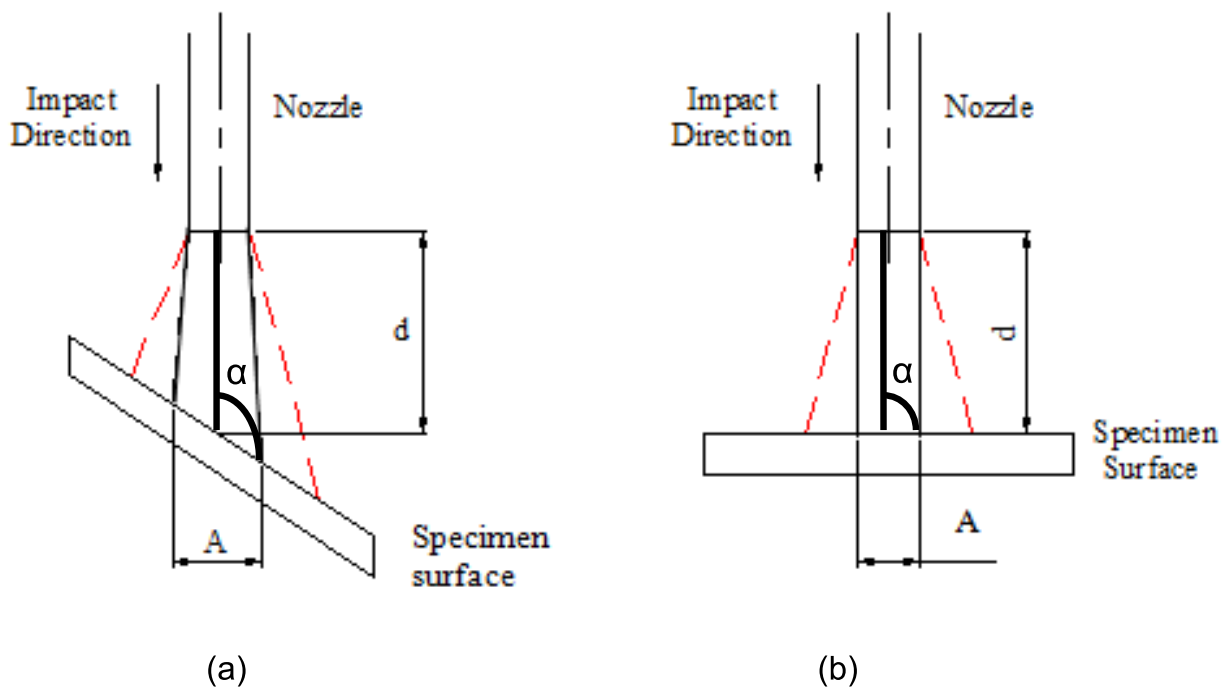
Figure 5. Impact geometry, (a) $\alpha \leq 45^\circ$, (b) Near or at 90°

Figure 6a-j present the wear mechanisms involved in this study on 4140 and 1018 steel and stainless steels 304, 316 and 420. In respect to AISI 4140, larger craters are clearly seen on the surface at 30° with some wear debris inside, whereas a more roughened surface is observed at 90°. AISI 1018 exhibited cracks located at random positions and also pitting action was seen on the surface at 45°. On the other hand, stainless steels 304, 316 and 420 showed pitting and ploughing action, irregular indentations, scratches and smeared wear debris at 30° and 45° whereas fragments of abrasive particles embedded or smeared on the surface were clearly seen at angles near or at 90°.

Photographs shown in Figure 7a- present the damage incurred on 6061 aluminium, copper and brass at different incident angles. Figure 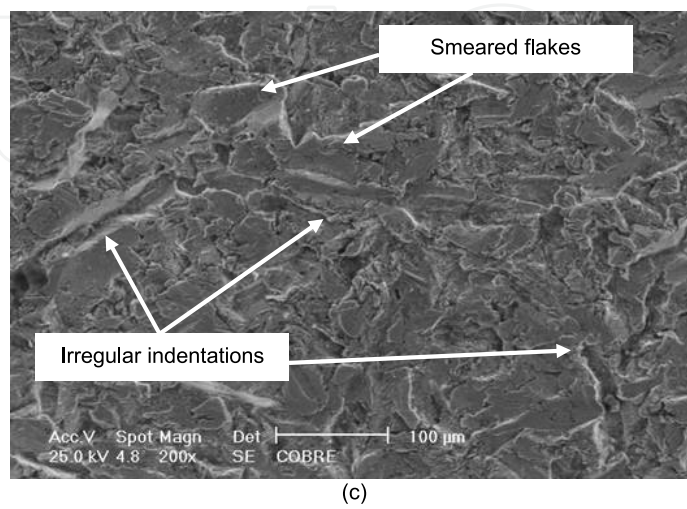7a shows the worn surface of aluminium; particles of aluminium debris and lips around the craters smeared by subsequent impacts of abrasive particles are observed as in other erosion studies [19-23]. Also, craters, pitting and striations are observed on the specimen surface. The reduction in mass loss at higher impact angles, near or at 90º, is because there was not too much evidence of sliding action of abrasive particles unlike lower impact angles where the sliding component is significant and increases the mass lost in the material. In addition, although a low particle velocity and abrasive flow rate were used to conduct the experiments, a higher interaction between incoming and rebounding particles in the region between the nozzle and target was seen since this phenomenon is normally increased at higher impact angles ($\alpha > 45^\circ$) as mentioned in previous studies conducted by other investigators [24-26]. The wear damage was characterized by a higher plastic deformation in the central part (primary erosion area). Small pits and craters of up to 50-70 µm in size were observed.
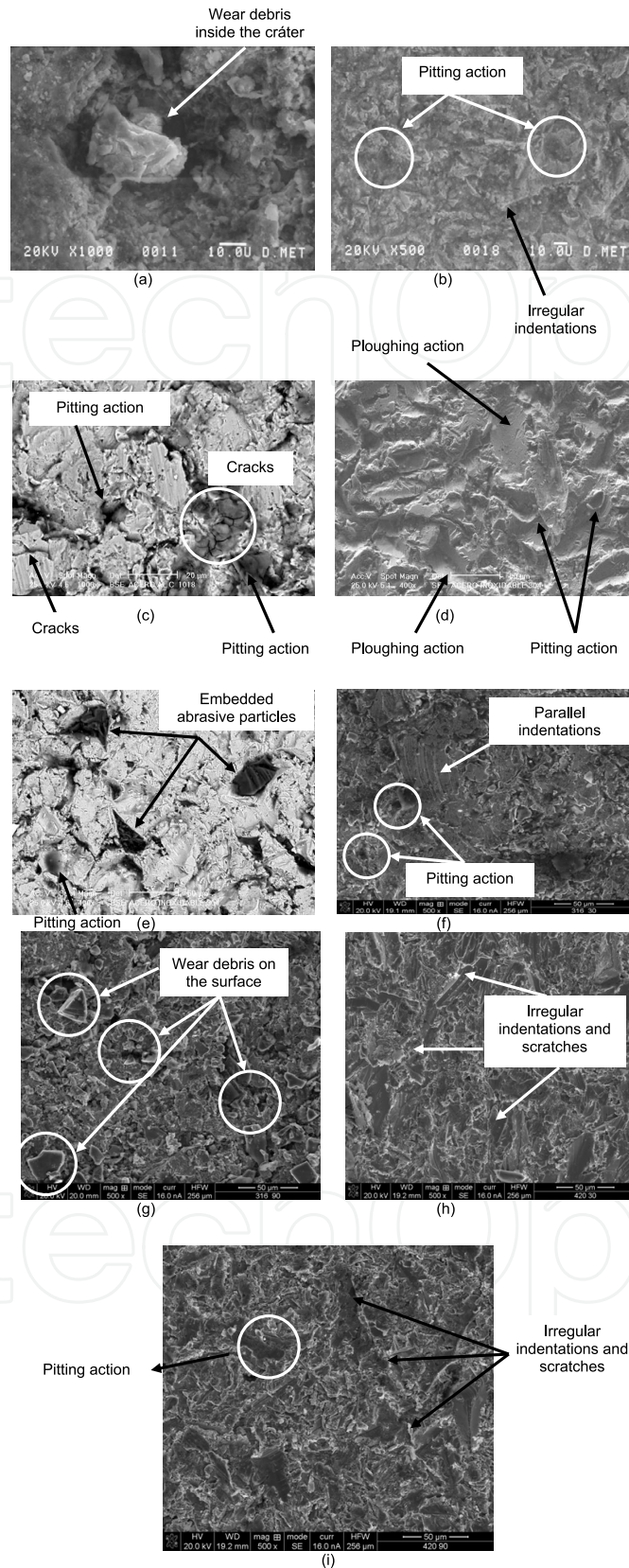
Figure 6. SEM photographs, (a) AISI 4140 at 30°, (b) AISI 4140 at 90°, (c) AISI 1018 at 45°, (d) Stainless steel 304 at 30°, (e) Stainless steel 304 at 90°, (f) AISI 316 at 30°, (g) AISI 316 at 90°, (h) AISI 420 at 30°, (i) AISI 420 at 90°.

Wear debris

Striations

Pitting action

(a)

Flattened material   Cráters

Ploughing action

Pitting action

Pitting action

(b)

Smeared flakes

Irregular indentations

(c)
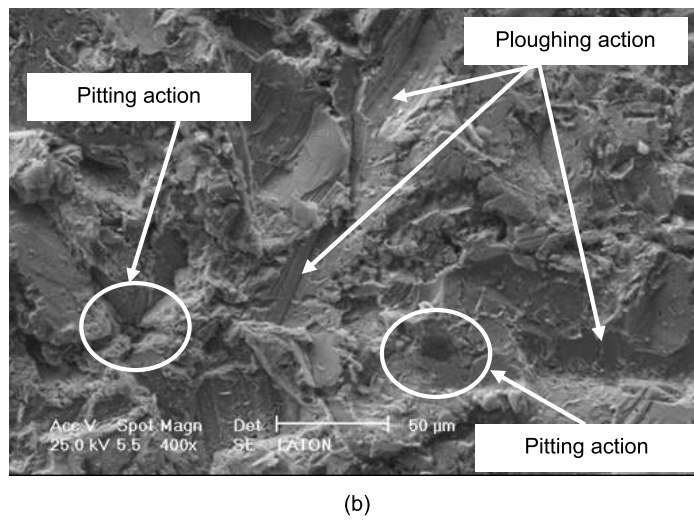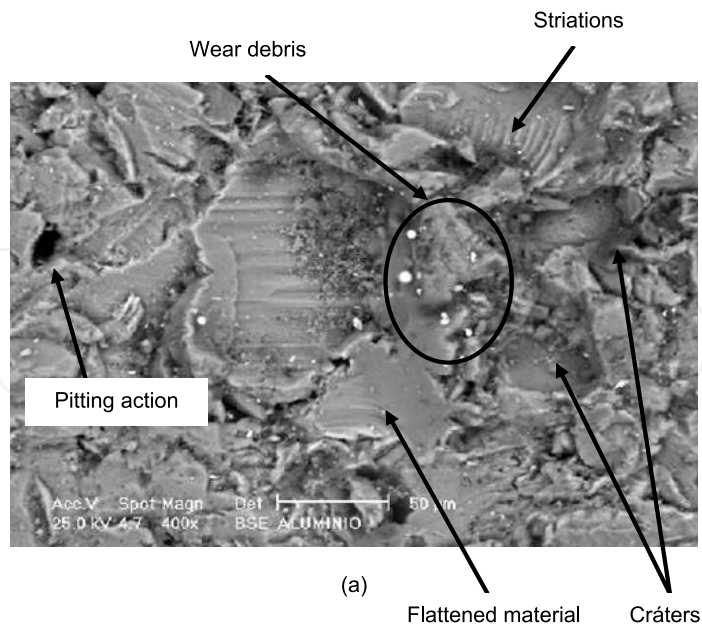
Figure 7. Erosion damage (a) 6061 Aluminium at 90°, (b) Brass at 45°, (c) Copper at 45°

A common occurrence characterized by grooves with material piled up to the sides due to the ploughing action of the particles was observed in brass (Figure 7b). The lips at the sides of the grooves had been flattened due to successive impacts of the erodent particles as exhibited in other studies on metallic materials. In the particular case at 45º (low impact angle), the sliding component played an important role in increasing the mass loss significantly, generating a ploughing action as commonly seen in previous erosion studies. Also, it was possible to see a pitting action which was thought to occur due to abrasive particles that only indented and did not slide on the material surface. Additionally, there is evidence of material separated in form of flakes and elongated parts that were flattened on the copper surface by the subsequent battering of the abrasive particles (Figure 7c) as presented in other erosion experiments [1-4].

Table 3 presents the results obtained of the mass loss at all the incident angles. Additionally, Figure 8 displays a graph of the total erosion rate against the impact angle, where most the erosion rates increases as the angle of impact was decreased. The total erosion rate was obtained by dividing the total mass loss after 10 min of each tested material by the total mass of the erodent hitting the specimen after this time. Most the materials displayed a ductile behaviour as their maximum erosion rate was reached at 30º and 45º and reduced considerably near or at 90º. It is assumed that this initial increase is because of a first group of particles that caused a cutting action on the material surface. In this particular case, the sliding component normally observed at lower impact angles caused severe problems. AISI 304 and 316 exhibited the poorest erosion resistance in comparison with all the tested materials. This behavior was not expected, however the results are very clear. In fact, the maximum erosion rate in these particular cases was reached at 60°, which is not common. Generally, in previous erosion studies on stainless steels, the higher erosion rates are seen at lower impact angles ($\alpha \leq 45°$). It is assumed that the room temperature could be a significant fact to modify the performance of these stainless steels. On the other hand, AISI 420 exhibited a normal behavior, showing its maximum erosion rate at 30°.

Impact angle (α)	AISI 4140	AISI 1018	AISI 304	AISI 316	AISI 420	6061 Al	Brass	Copper
30°	0.0741	0.1372	0.6928	0.5625	0.1011	0.0502	0.1656	0.1119
45°	0.0657	0.1066	0.5803	0.7021	0.0683	0.0471	0.1752	0.1024
60°	0.057	0.0771	1.0875	0.8897	0.0895	0.0455	0.1569	0.0885
90°	0.0536	0.0206	0.7755	0.7398	0.0743	0.0361	0.1103	0.0695

Table 3. Mass loss at different incident angles

The behavior observed in most materials used to conduct this study was as expected because these typically display a maximum erosion rate at lower incident angles and the damage is significantly reduced as the impact angle is increased. It is assumed that the materials used in this study exhibited ductile type behavior. This trend is commonly seen in the graphs used in previous erosion studies, as illustrated in Figure 9 [4].
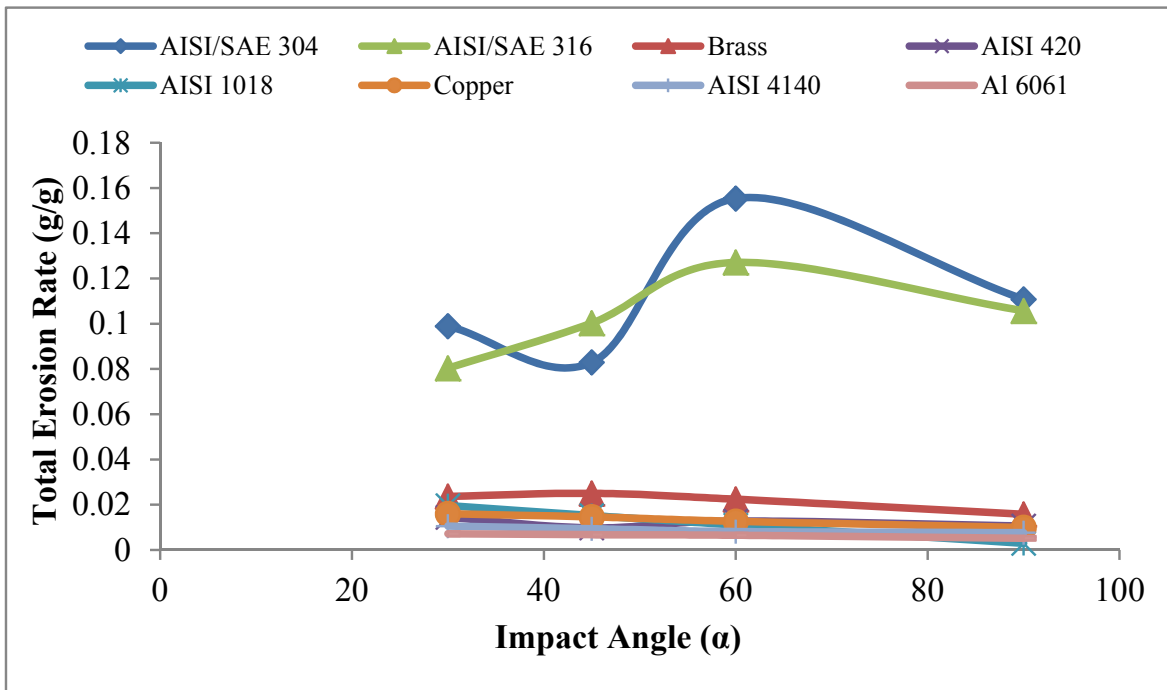
Figure 8. Total erosion rate against impact angle
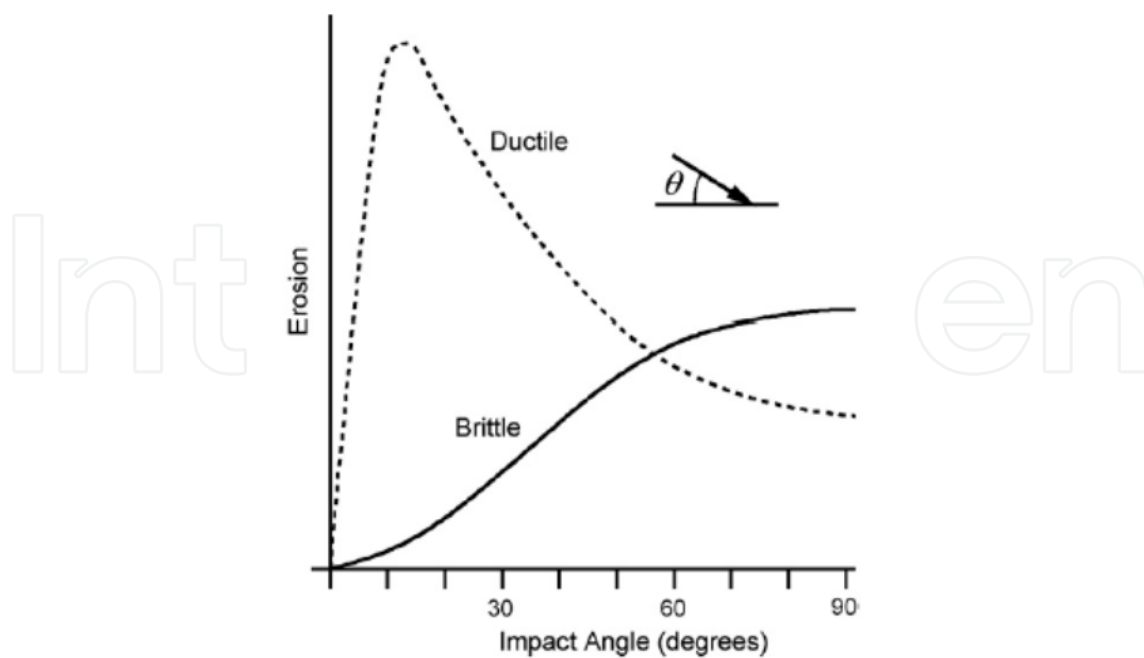

Figure 9. Erosive wear rates for brittle and ductile materials [4].

4. Conclusions

- Aluminium 6061 was the material that exhibited the higher erosion resistance whereas stainless steels 304 and 316 showed the poorer performance against this wear process. It was assumed that the room temperature could have affected the behavior of these materials.

- Most the tested materials exhibited a ductile type behavior due to their maximum erosion rate was reached at lower impact angles (30° and 45°). The erosion rate was considerably decreased at higher incidence angles (60°, 75° and 90°). Stainless steels 304 and 316 had higher erosion damage at 60°.

- Typical wear mechanisms such as ploughing and pitting action, irregular indentations, scratches, craters, embedded abrasive fragments, smeared wear debris on the surfaces and brittle fracture characterized by cracks located at random positions were observed in this particular study.

- The wear scars were characterized by an elliptical shape at 30° and 45°, which is a characteristic feature when the specimens are impacted at low-impact angles ($\alpha \leq 45°$), whereas a nearly circular shape was observed at 60° and 90°.

Author details

Juan R. Laguna-Camacho*
Universidad Veracruzana, Faculty of Electric and Mechanical Engineering,
Poza Rica de Hidalgo, Veracruz, México

M. Vite-Torres and E.A. Gallardo-Hernández
2SEPI, ESIME, IPN, Unidad Profesional "Adolfo López Mateos"
Tribology Group, Mechanical Engineering Department, México, D.F.

E.E. Vera-Cárdenas
Universidad Politécnica de Pachuca, Pachuca, México

5. References

[1] Venkataraman B. & Sundararajan G., The Solid Particle Erosion of Copper at Very Low Impact Velocities, Wear 1989; 135, 95-108.

[2] Ambrosini L. & Bahadur S., Erosion of AISI 4140 Steel, Wear 1987; 117, 37-48.

[3] Harsha A. P. & Deepak Kumar Bhaskar, Solid Particle Erosion Behavior of Ferrous and Non-ferrous Materials and Correlation of Erosion Data with Erosion Models, Materials and Design 2008; 29, 1745-1754.

[4] Hutchings I. M., Tribology: Friction and Wear of Engineering Materials, London, Edward Arnold; 1992.

---

* Correspondig Author

[5] Morrison C.T. & Scattergood R. O., Erosion of 304 stainless steel, Wear 1986; 111, 1-13.

[6] Levy A. V. & Chik P., The Effects of Erodent Composition and Shape on the Erosion of Steel, Wear 1983; 89, 151-162.

[7] Liebhard M. & Levy A., The Effect of Erodent Particle Characteristics on the Erosion of Metals, Wear 1991; 151, 381-390.

[8] Laguna-Camacho J. R., Development of a prototype for erosion testing using compressed air and abrasive particle flow, Master Thesis, SEPI–ESIME-UZ– IPN, México; 2003.

[9] ASTM standard, G76-95 (1995), Standard practice for conducting erosion tests by solid particle impingement using gas jets, in Annual Book of ASTM Standards, Vol. 03.02, ASTM, Philadelphia, PA, 1995: pp. 321-325.

[10] Vite J., Vite M., Castillo M., Laguna-Camacho J. R., Soto J., Susarrey O., Erosive Wear on Ceramic Materials Obtained from Solid Residuals and Volcanic Ashes, Tribology International 2010; 43, 1943-1950.

[11] Kosel T. H. and Anand K., An Optoelectronic Erodent Particle Velocimeter, in V. Srinivasan and K. Vedula (eds.), Corrosion and particle erosion at high temperature, The minerals, Metals and Materials Society 1989; 349-368.

[12] Shipway P. H. & Hutchings I. M, Influence of Nozzle Roughness on Conditions in a Gas-Blast Erosion Rig, Wear 1993; 162-164, 148-158.

[13] Laguna-Camacho, J. R., A study of erosion and abrasion wear processes caused during food processing, PhD thesis, The University of Sheffield, UK; 2009.

[14] Finnie I., Some Observations on the Erosion of Ductile Metals, Wear 1972; 19, 81-90.

[15] Finnie I., Stevick G. R., Ridgely J. R., The Influence of Impingement Angle on the Erosion of Ductile Metals by Angular Abrasive Particles, Wear 1992; 152, 91-98.

[16] Camacho J., Lewis R., Dwyer-Joyce R. S., Solid Particle Erosion Caused by Rice Grains, Wear 2009; 267, 223-232.

[17] Laguna-Camacho J. R., Cruz-Mendoza L. A., Anzelmetti-Zaragoza J. C., Marquina-Chávez A., Vite-Torres M., Martínez-Trinidad J., Solid Particle Erosion on Coatings Employed to Protect Die Casting Molds, Progress in Organic Coatings 2012; 74, 750-757.

[18] Lapides L., Levy A., The Halo Effect in Jet Impingement Solid Particle Erosion Testing of Ductile Metals, Wear 1980; 58, 301-311.

[19] Hutchings I. M., Winter R. E., Particle Erosion of Ductile Metals: A Mechanism of Material Removal, Wear 1974; 27, 121-128.

[20] Winter R. E., Hutchings I. M., Solid Particle Erosion Studies Using Single Angular Particles, Wear 1974; 29, 181-194.

[21] Tilly G. P., A Two Stage Mechanism of Ductile Erosion, Wear 1973; 23, 87-96.

[22] Tilly G. P., Wendy Sage, The Interaction of Particle and Material Behavior in Erosion Processes, Wear 1970; 16, 447-465.

[23] Bellman R., Levy A., Erosion Mechanisms in Ductile Metals, Wear 1981, 70, 1-27.

[24] Rickerby D. G., Macmillan N. H., The Erosion of Aluminium by Solid Particle Impingement at Normal Incidence, Wear 1980; 60, 369-382.

[25] Shipway P. H., Hutchings I. M., A Method for Optimizing the Particle Flux in Erosion Testing with a Gas-Blast Apparatus, Wear 1994; 174, 169-175.

[26] Anand K., Hovis S. K., Conrad H., Scattergood R. O., Flux Effects in Solid Particle Erosion, Wear 1987; 118, 243-257.